DINSAR EXPERIMENTS FOR SHANGHAI GROUND SUBSIDENCE MONITORING BY USING ALOS PALSAR DATA

PI395

Jicang Wu[1], Lina Zhang[1], Baosong Ban[1], Tao Li[1], Caijun Xu [2], Yamao Wen [2]

[1] Department of Surveying and Geo-Informatics, Tongji University, 1239 Siping Road, Shanghai, 200092, China, jcwu@tongji.edu.cn

[2] School of Geodesy and Geomatics, Wuhan University, 129 Luoyu Road, Wuhan, 430071, China, cjxu@sgg.whu.edu.cn

The Advanced Land Observing Satellite (ALOS) PALSAR data is used to take two pass interferometry for extraction of ground subsidence in Shanghai China. At first a set of two pass interferometry with baseline less than 1km are taken and corresponding coherence factor are used to indentify persistent scatterers (PS) so as to form a time series of differential phase of every PSs. A linear subsidence model is applied at all PS points and the subsidence rates of all PSs are obtained through a stacking of the time series. The obtained subsidence rates are calibrated with existing leveling results and show a good agreement with the leveling. In addition, a strip area including the Shanhai maglev line is chosen for similar DInSAR processing to extract ground subsidence nearby.

Keywords: InSAR, ALOS PALSAR, stacking, persistent scatterers, ground subsidence

1. INTRODUCTION

Ground subsidence has become a major geological disaster in Shanghai, as a result of underground water extraction and huge engineering constructions such as undergrounds, skyscrapers [1]. Therefore, a variety of methods have been used to monitor ground subsidence. Conventional high precision leveling has been used for monitoring ground subsidence since 1921 [2]. A GPS network composed more than 34 stations have been build up since 2002 with an annual campaign surveying [3]. In recent years, InSAR technology, for its larger area coverage, high spatial resolution, all weather running, cheap cost, and automatic operations, has also been used for monitoring Shanghai ground subsidence [4]. In this research we aim to apply ALOS PALSAR data to extract ground subsidence information in Shanghai downtown area.

ALOS PALSAR is an L-band synthetic aperture radar. Its wavelength is 23.6 cm, which has the following capacity over C-band SAR such as Envisat and ERS 1/2: (1) deeper penetration of vegetated areas results in less temporal decorrelation; (2) longer critical baseline results in more usable interferometric pairs. In addition, PALSAR is operated in some different modes that could enhance the interferometric capabilities [4].

In the following, we first introduce the methodology for two pass interferomety and extraction of ground subsidence rates based on time series of interferometric phases of persistent scatterers. Then the ground subsidence rates are estimated based on the PALSAR data from 2007 to 2009 .

2. METHODOLOGY

By taking two pass interferometry, the observed interferometric phase difference ϕ can be written as follows:

$$\phi = \phi_{def} + \phi_{dem} + \phi_{orb} + \phi_{trop} + \phi_{noise} \quad (1)$$

where ϕ_{def} is the phase related to ground deformation, ϕ_{dem} is the phase caused by DEM errors, ϕ_{orb} is the residual orbital phase, ϕ_{trop} is the phase related to atmospheric delay, and ϕ_{noise} is random noise due to various reasons.

For overcoming the orbit and atmospheric errors, a polynomial fitting is applied to remove the trend errors from orbit and atmosphere [5][6]. External DEM is required for two-pass DInSAR to eliminate the topographic affects in the interferometric phases [7]. Here, the Shuttle Radar Topography Mission (SRTM) 3 arc DEM products [8] is used for topographic correction in all two pass interferometries.

.

2.1 POLYNOMIAL FITTING

As mentioned above, for the linear systemic errors such as orbit errors, the polynomial fitting method is applied to fit the errors. We suppose that the deformation between the two SAR images is very small so that it can be ignored to some extent. Then the residual orbital error can be expressed as:

$$\phi_{orb} = ax + by + cxy + d \quad (2)$$

where x, y are pixel coordinates in range and azimuth respectively. Using the least squares method, the parameter $[a \quad b \quad c \quad d]$ can be acquired and the residual orbital phase is estimated. Actually the linear part of atmospheric error is also be eliminated by this polynomial fitting, On the other hand, we should not use the whole image pixels for the polynomial fitting, only the persistent scatterer points with high coherence are chosen [9].

2.2 INTERFEROGRAM STACKING

After taking the polynomial fitting, atmospheric delay, especially tropospheric delay can be regarded as random signal. The influence of tropospheric delay in the interferometric phases can be reduced by stacking the series of interferograms, and the average linear deformation rate can be acquired. Suppose we have *N* interferometric pairs, phase ϕ_i is acquired between two SAR images with time interval t_i (in unit of year), and then the phase rate can be expressed as:

$$v_i = \frac{\phi_i}{t_i} \quad (3)$$

Suppose the surface deformation is linear, a model can be formed:

$$\phi_i = \bar{v} \cdot t_i \quad (4)$$

To get credible results, we only choose the persistent scatterer points of high coherence. Define the average coherence coefficient as

$$\bar{\gamma} = \frac{1}{N} \sum_{i=1}^{N} \gamma_i \quad (5)$$

where γ_i is the coherence coefficient of a pixel in the *i*th interferogram. A threshold is chosen and the point will be used as the persistent scatterer only when $\bar{\gamma}$ is larger than the threshold.

Further, we set γ_i as the weight of the interfermetric phase in the least squares estimation, and we get the phase rate as:

$$\bar{v} = \sum_{i=1}^{N} \gamma_i \cdot \phi_i \cdot t_i / \sum_{i=1}^{N} \gamma_i \cdot t_i^2 \quad (6)$$

And the standard error is

$$\sigma = \sqrt{\frac{1}{N} \sum_{i=1}^{N} \left(\phi_i - \bar{v} \cdot t_i \right)^2} \quad (7)$$

3. PALSAR INTERFEROMETRY EXPERIMENT

3.1 THE SHANGHAI DOWNTOWN AREA

In this paper we us 13 scenes of ALOS PALSAR 1.0 repeat-path data (Path No. 441, Frame 610) covering Shanghai area, from February 2007 to April 2009. Fig. 1 shows the geocoded image of the frame. For speeding the data processing, only the downtown area (see white box in Fig. 1, about 180km^2) are chosen for this study. At first all the FBD mode image are oversampled to keep the same sampling rate as the FBS mode, and then interferograms are taken one by one using JPL/Caltech ROI_PAC software [10]. With the limit of the baseline less than 1km, 27 interferomgrams are obtained and the corresponding master and slave images with spatial and temporal baseline lengths are listed in Table 1. After taking earth curvature and topographic correction with external STRM EDM, the wrapped interferometric phase images are obtained. Fig. 2 shows all the 27 interferograms. We can see that three of them (071125-080527,080110-080527, 080225-080527) have abrupt changes. Considering the three temporal baseline less than 1 year and the ground subsidence is subtle, these abrupt changes are thought to be the effects of the atmospheric delay, properly related to the bad weather of the common slave image. So in the following data processing, these three interferograms are not included.

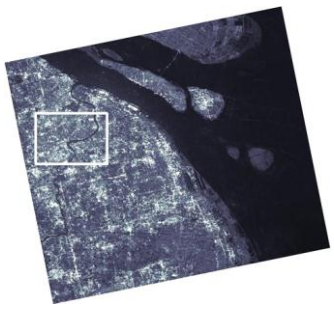

Fig.1 Geocoded image of frame 610 path 441. The white rectangle indicates the region of test area.

Table 1 Information of interferometric pairs

No.	Master	Slave	Bp (m)	Bt (day)
1	20070222	20070825	- 779	184
2	20070222	20080712	422	506
3	20070222	20090227	950	736
4	20070222	20090411	95	782
5	20070825	20071125	-545	92
6	20070825	20080110	-657	138
7	20070825	20090411	873	230
8	20071125	20080110	-112	46
9	20071125	20080225	-655	92
10	20071125	20080527	-841	184
11	20080110	20080225	-542	46
12	20080110	20080411	-941	92
13	20080110	20080527	-729	138
14	20080225	20080411	-399	46
15	20080225	20080527	-187	92
16	20080411	20080527	213	46
17	20080712	20090112	604	184
18	20080712	20090227	528	230
19	20080712	20090414	-327	276
20	20081012	20081127	-221	46
21	20081012	20090112	-673	92
22	20081012	20090227	-748	138
23	20081127	20090112	-452	46
24	20081127	20090227	-527	92
25	20090112	20090227	-75	46
26	20090112	20090411	-931	92
27	20090227	20090411	-856	46

On the other hand, considering the chosen area is quite small, the ground subsidence is subtle for the period of each interferogram, the phase unwrapping is not necessary to be taken, the possibility of existing ambiguity points are deleted as the blunder errors. By setting the minimum correlation threshold as 0.25 and minimum average correlation threshold as 0.45, 27,415 points are indentified as the persistent scatterers (PS density is about 300/km^2). After taking polynomial fitting, interferogram stacking is used for extraction of linear subsidence rate and EDM error at each PS, see Fig. 3 for the results obtained. The relative subsidence rate is less than 10mm/a. The EDM error is less than 10m which reflects the stated precision of SRTM EDM products.

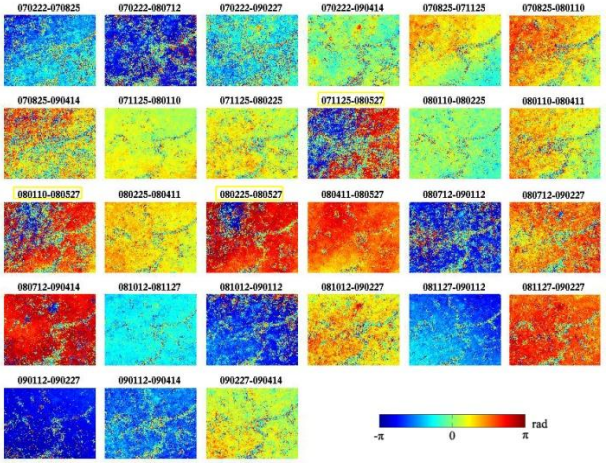

Fig. 2 Wraped interferogram of the downtown area

The ground subsidence rates obtained above are relative to a reference point (the triangle point in Fig.3), the absolute subsidence rate is not available. So we chose the existing 9 leveling benchmarks in the downtown area with known subsidence rates to calibrate the ground subsidence rates obtained by interferograms. Fig. 4 shows the distribution of the 9 benchmarks in the area. At first, the differences of ground subsidence rates between the PSs to the nearest benchmarks are used to calculate the calibration value:

$$C_{calibration} = \frac{1}{9}\sum_{i=1}^{9} C_i \quad \text{, and}$$

$$C_i = v_{keveling} - v_{CP} \qquad (8)$$

where $v_{leveling}$ is the known ground subsidence rate obtained by the repeated high precision leveling and v_{CP} is ground subsidence rate of corresponding nearest PS (the LOS rate has been reduced to vertical rate in advance).

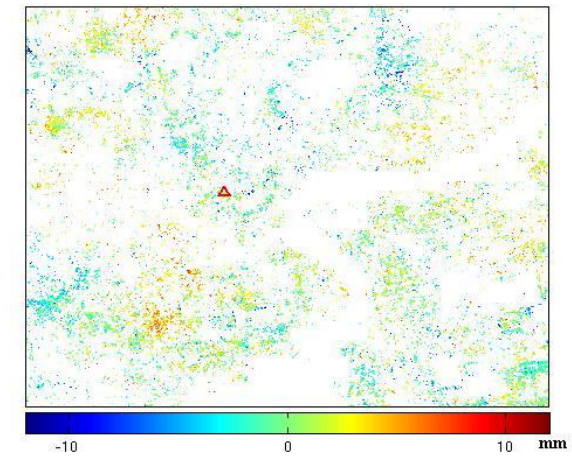

Fig. 3 Relative ground subsidence rate and EDM error (The red triangle is the reference point. Top: ground subsidence rate and bottom EDM error)

Fig. 4 Test area in Google earth and distribution of leveling benchmarks (the triangles). The green one is chosen as reference point for interferometry.

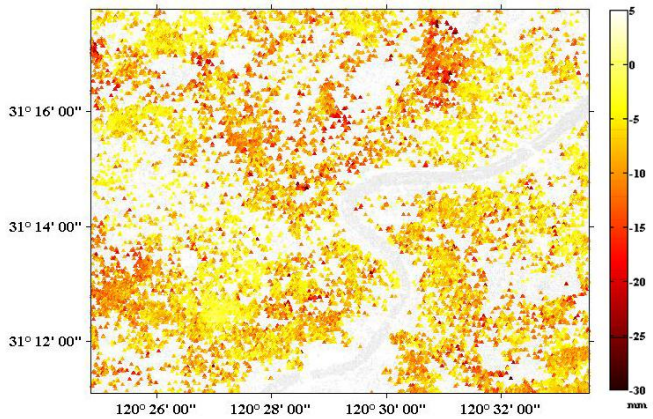

Fig. 5 Calibrated ground subsidence rate of PSs

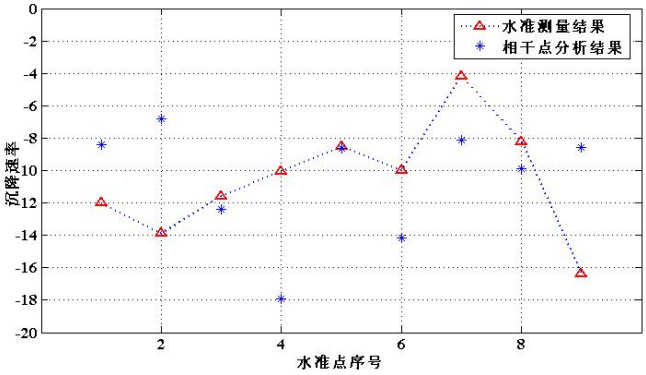

Fig.6 The differences of ground subsidence rate between PS and corresponding benchmark

Fig. 5 is the calibrated ground subsidence rate of all PSs. Most of the downtown area has no significant ground subsidence with subsidence rate less than -5mm/a. And there some places with local subsidence rate greater than 10mm/a. The maximum subsidence rate is located in the upper right of Fig.5 and with a value of about -30mm/a, where is the south of Yangpu district. Fig. 6 shows the difference between calibrated ground subsidence rates of PSs with that of corresponding leveling benchmarks. There are 3 points with the differences larger than 7mm/a and the differences of the other 6 points are all within 4mm/a to show a good agreement with the subsidence rates from the leveling.

3.2 THE SHANGHAI MAGLEV

The running of Shanghai maglev requires a stable ground support bases. We applied ALOS PALSAR data to study the ground subsidence along the maglev zone. Based on the similar procedures as in 3.1, eight PALSAL images covering the Maglev zone during 2007 to 2008 have been used to form 7 interferograms using DInSAR method. Table 2 lists the parameters of the 7 interfeometric pairs. The maximum spatial baseline is less than 600, and the time separations are all 46 days.

Tab.2 Information of interfeometric pairs

No.	Master	Slave	Bp(m)	Bt(day)
IP1	20070710	20070825	-124	46
IP2	20070825	20071010	-280	46
IP3	20071010	20071125	-273	46
IP4	20071125	20080110	-117	46
IP5	20080110	20080225	-549	46
IP6	20080225	20080411	-403	46
IP7	20080411	20080527	210	46

For taking a case study, two profiles across the maglev have been chosen for extraction of ground subsidence rates. And the relative subsidence velocity of the two profiles obtained by the stacking method. Fig.7 shows the relative subsidence rates along the two profiles. In Fig.7, the middle point is on the rail and chosen as the reference point, and each 20 points on left and right side of the rail are chosen to draw the profile. We can see that a tendency of subsidence uniformly distributed on both side of the maglev, indicating higher stability of basement of the maglev. More details can be found in [11].

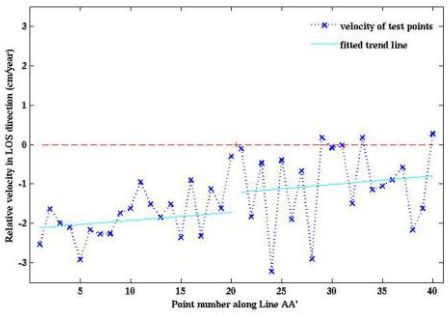

(a)

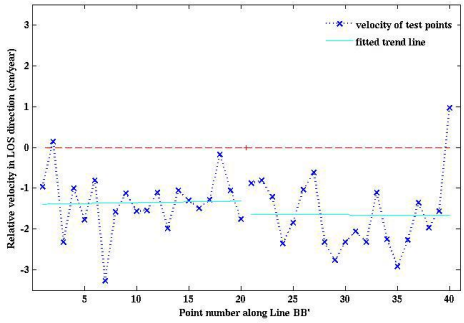

(b)

Fig.7 Relative LOS displacement rates of the points along the two test profiles

4. CONCLUSIONS

Two pass SAR interferogrammetry with selected spatial and temporal baselines are used to get the time series of LOS displacements of PSs and further applied to extract of ground subsidence rates. 13 PALSAR images from February 2007 to April 2009 in Shanghai area are used for extraction of the linear ground subsidence rates at the downtown area. The results show that the most places of the downtown area have no significant subsidence. There are some places with significant local subsidence rates at about -10mm/a or even more. The maximum ground subsidence rate is -30mm/a which locates at the south of Yangpu district. In addition, 8 PALSAR images covering the Shanghai maglev are used for study the ground stability along the rail. According to the two chosen profiles, the result shows that the ground basis of the Shanghai maglev is quite stable.

Acknowledgment

The work in this paper is supported by National Natural Science Foundation of China (40674004). We thank JAXA for providing PALSAR data. We thank JPL/Caltech for providing ROI_PAC software.

REFERENCES

[1] Qingfen Li and Hanmei Wang, “A Study on Land Subsidence in Shanghai”, Geological Journal of China Universities, Vol.12, No.2, June 2006, pp. 169-178. (in Chinese)

[2] AGen Zhang, "Sustainable development and land subsidence controlling management in shanghai", The Chinese Journal of Geological Hazard and

Control, Vol. 16, No. 1, Mar. 2005, pp. 1-4. (in Chinese)
[3] Shuli Song, Wenyao Zhu, Jincai Ding and Zongyi Cheng, “Primary Results Monitored by SGCAN and the Application Future”, Chinese Journal of Nature, Vol. 26, No. 2, 2004, pp. 118-121. (in Chinese)
[4] D. T. Sandwell, D. Myer, R. Mellors and M. Shimada, “Accuracy and Resolution of ALOS Interferometry: Vector Deformation Maps of the Father’s Day Intrusion at Kilauea”. IEEE Transactions on Geoscience and Remote Sensing, Vol. 46, No. 11, 2008, pp. 3524-3534
[5] Lei Zhang, Jicang Wu, Xiaoli Ding, Feng Xiao, "The propagation of orbital errors in the 3-Pass DInSAR processing," in Proceeding of 2007 1st Asian and Pacific Conference on, vol. Synthetic Aperture Radar, pp. 5-9
[6] H, Zebker, P. A., Rosen and S Hensley. “Atmospheric Effects in Interferometric Synthetic Aperture Radar Surface Deformation and Topographic Maps”, J. Geophys. Res., 1997, 102 (B4), pp. 7 547-7 563
[7] T. Strozzi, U. Wegmüller, L. Tosi, G. Bitelli, and V. Spreckels, “Land subsidence monitoring with differential SAR interferometry”, Photogrammetric engineering and remote sensing, Vol. 67, No. 11, Nov. 2001, pp. 1 261–1 270
[8] T. G. Farr, M. Kobrick, “Shuttle Radar Topography Mission produces a wealth of data”, EOS Trans. AGU, 2000, 81, pp. 583-585
[9] Mario Costantini, Salvatore Falco, Fabio Malvarosa, Federico Minati, “ A new method for identification and analysis of persistent scatterers in series of SAR images”, in Proc. Int. Geosci. Remote Sensing Symp (IGARSS), Boston MA, USA, 7-11 July 2008, pp. 449-452.
[10] P. A. Rosen, S. Hensley, G. Peltzer, M. Simons, “Updated Repeat Orbit Interferometry Package Released”, Eos Trans. AGU, 2004, 85(5).
[11] Wu, J., S. Hu, S. Ji, and R. Liu, “Monitoring ground subsidence along the Shanghai maglev zone using ALOS PALSAR data”, International Workshop, Spatial Information Technologies for Monitoring the Deformation of Large-Scale Man-made Linear Features, Jan.10-11, 2010, Hong Kong.